

Multiphoton resonances in nitrogen-vacancy defects in diamond

Sergei Masis, Nir Alfasi, Roei Levi, Oleg Shtempluck, and Eyal Buks

Andrew and Erna Viterbi Department of Electrical Engineering, Technion, Haifa 32000, Israel



(Received 12 December 2018; published 25 July 2019)

Dense ensembles of nitrogen-vacancy (NV) centers in diamond are of interest for various applications, including magnetometry, masers, hyperpolarization, and quantum memory. All of the applications above may benefit from a nonlinear response of the ensemble, and hence multiphoton processes are important. An enhancement of the multiphoton response is demonstrated by coupling the NV ensemble to a superconducting cavity. Moreover, the measured multiphoton response of the NV ensemble exhibits a regular pattern, which suggests that a dipolar coupling to nitrogen-14 substitutional defects (P1) plays a role in this process. As an example of an application, increased responsivity to magnetic field is demonstrated.

DOI: [10.1103/PhysRevA.100.013852](https://doi.org/10.1103/PhysRevA.100.013852)

I. INTRODUCTION

A two-level system (TLS) is perhaps the most extreme manifestation of nonlinear response. Systems composed of TLSs and other elements exhibit a variety of nonlinear dynamical effects, including multiphoton resonances (MPRs) [1–4], frequency mixing [5–7], fluorescence [8,9], dynamical instabilities [10,11], suppression of tunneling [12,13], and breakdown of the rotating-wave approximation [14].

Here we study nonlinear response of an ensemble of nitrogen-vacancy (NV) defects in diamond [15]. Two mechanisms that allow the enhancement of MPR are explored. The first one is based on an electromagnetic cavity mode that is coupled to the spin ensemble [16–23]. The second one is attributed to hyperfine splitting [24] of P1 defects [25–27] and their dipolar coupling to the negatively charged NV defects (NV⁻).

The NV⁻ defect has a spin-triplet ground state [28] with a relatively long coherence time [29]. The NV⁻ spin state can be initiated via the process of optically induced spin polarization (OISP) [30,31] and can be measured using the technique of optical detection of magnetic resonance (ODMR) [32–34]. These properties facilitate a variety of applications, including magnetometry [26,35–41], sensing [29,36,42,43], and quantum information processing [44,45].

Dipolar coupling between NV⁻ and other spin species in diamond gives rise to intriguing effects, including hyperpolarization [46–49] and cross relaxation [27,50,51], and can be exploited for optical detection of spin defects in diamond other than NV⁻ [25,52–57].

The process of cross polarization between NV⁻ and P1 defects plays an important role in the MPR mechanism. In general, the efficiency of cross polarization depends on the rate of a competing effect of thermal polarization, which is characterized by the longitudinal spin-relaxation rate. At cryogenic temperatures the thermal polarization rate can be significantly reduced, and consequently, the efficiency of cross polarization is enhanced.

II. LOW-MAGNETIC-FIELD ODMR

A spiral resonator [58] made of 500-nm-/10-nm-thick niobium/aluminum with an inner radius of 0.7 mm and linewidth and spacing of 20 μm is fabricated on a sapphire substrate. Type-Ib [110] diamond is irradiated with 2.8 MeV electrons at a dose of 8 × 10¹⁸ e/cm², annealed for 2 h at 900 °C and acid cleaned. The sample assembly (see Fig. 1) is placed at a cryostat with a base temperature of 3.6 K and mechanically aligned along the magnetic field of an external superconducting solenoid. The photoluminescence light passes through an array of filters and is collected by a photodiode. A microwave synthesizer is connected directly to a loop antenna (shortened end of a coaxial cable) mounted below the sapphire substrate, and the signal amplitude is 100% modulated with a low-frequency sine wave. The same wave is used for the photodiode signal demodulation by a lock-in amplifier. Microwave reflection measurements of the resonator yield resonance frequency $\omega_c = 2\pi \times 276$ MHz, unloaded quality factor $Q = 96$, and critical temperature $T_c = 7$ K. The rather low Q might be explained by the proximity to irradiated diamond. The coupling coefficient g between the resonator and the NV⁻ ensemble is given by [23]

$$g^2 = \frac{\gamma_e^2 \mu_0 \hbar \omega_c \int d\mathbf{r} n_S P_z |\mathbf{B}_c|^2 \sin^2 \varphi}{\int d\mathbf{r} |\mathbf{B}_c|^2}, \quad (1)$$

where $P_z \approx 0.15$ [57] is the spin polarization, $n_S = 3 \times 10^{17}$ cm⁻³ is the NV⁻ ensemble number density, φ is the angle between the NV⁻ axis and the cavity magnetic field \mathbf{B}_c , μ_0 is the free-space permeability, and $\gamma_e = 2\pi \times 28.03$ GHz T⁻¹ is the electron-spin gyromagnetic ratio. Assuming constant P_z throughout the diamond, g is readily calculated by means of numerical simulation [see Fig. 1(b)] to be $g = 8$ MHz.

ODMR as a function of magnetic field and frequency is shown in Fig. 2. The lines marked by crosses in Fig. 2 are calculated by numerically diagonalizing the NV⁻ ground-state spin-triplet Hamiltonian, which is given by [59,60]

$$\frac{\mathcal{H}_{NV}}{\hbar} = \frac{DS_z^2}{\hbar^2} + \frac{E(S_+^2 + S_-^2)}{2\hbar^2} - \frac{\gamma_e \mathbf{B} \cdot \mathbf{S}}{\hbar}, \quad (2)$$

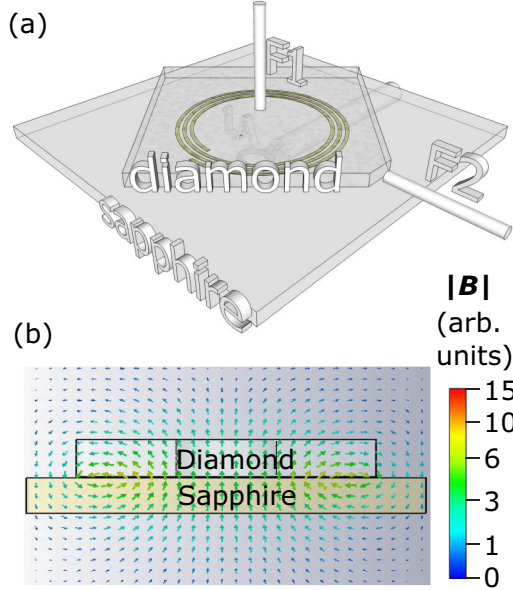


FIG. 1. (a) Experimental setup. The diamond is glued on top of the spiral resonator, and two multimode optical fibers, F1 and F2, are attached to the diamond top and side faces, respectively. A 532-nm-wavelength laser is introduced from one of the fibers, and the photoluminescence is collected from the other, providing a geometrical filtering of the laser light. A microwave loop antenna is placed below the sapphire at a location optimizing the resonator coupling. (b) CST studio simulation of the spiral fundamental mode magnetic field distribution.

where $\mathbf{S} = (S_x, S_y, S_z)$ is a vector spin $S = 1$ operator, the raising S_+ and lowering S_- operators are defined by $S_{\pm} = S_x \pm iS_y$, the zero-field splitting induced by spin-spin interaction D is given by $D = 2\pi \times 2.87$ GHz, the strain-induced splitting E is about $2\pi \times 10$ MHz for our sample, and \mathbf{B} is the externally applied magnetic field. The field \mathbf{B} has two contributions, $\mathbf{B} = \mathbf{B}_S + \mathbf{B}_L$, where \mathbf{B}_S (\mathbf{B}_L) is the stationary (alternating) field generated by the solenoid (the loop antenna) and is nearly parallel to the lattice direction $[111]$ ($[1\bar{1}0]$).

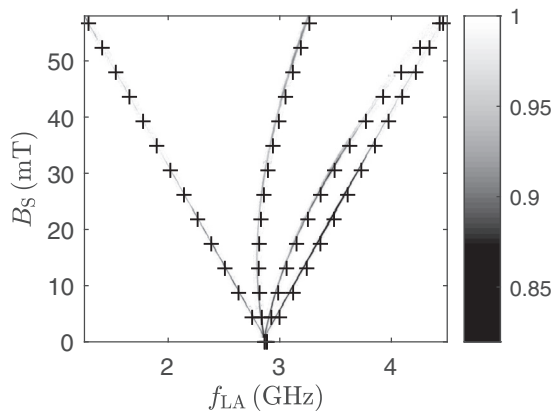


FIG. 2. Low-magnetic-field ODMR. The overlaid crosses are calculated by diagonalizing the NV^- spin Hamiltonian (2). The two nearly straight diagonal curves (leftmost and rightmost) correspond to the NV axis vector nearly parallel to the magnetic field, while the two remaining curves in the middle correspond to the nearly degenerate three other possible orientations of the NV axis vectors.

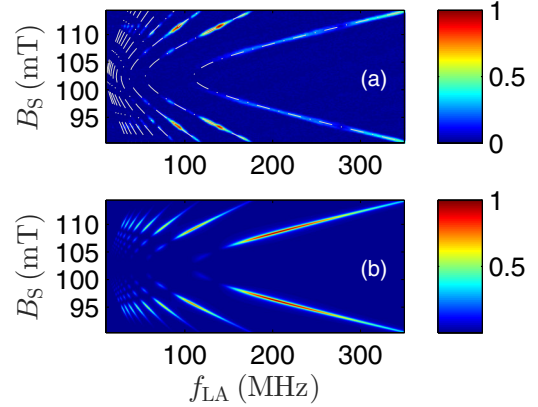


FIG. 3. ODMR with low laser power. (a) The normalized ODMR signal as a function of driving frequency f_{LA} and magnetic field B_S . The overlaid hyperbolas are calculated according to Eq. (3). (b) The normalized steady-state polarization $P_z/P_{z,s}$ is calculated according to Eq. (4) with the following parameters: $\omega_c = 2\pi \times 276$ MHz, $\gamma_c = 2.87$ MHz, $\gamma_1 = 20$ Hz, and $\gamma_2 = 30$ MHz. In terms of the parameter η the coupling coefficient β_{Δ} is expressed as $\beta_{\Delta} = \beta_{\Delta 0} \eta / \sqrt{1 + \eta^2}$, where $\beta_{\Delta 0} = 10$.

In a single-crystal diamond the NV centers have four different possible orientations. When hyperfine interaction is disregarded, each orientation gives rise to a pair of angular resonance frequencies ω_{\pm} , corresponding to the transitions between the spin state with magnetic quantum number 0 and the spin state with magnetic quantum number ± 1 . The line marked by crosses in Fig. 2 with the smallest (largest) frequency for any given magnetic field corresponds to the angular frequency ω_- (ω_+) of the NV^- defects with the axis in the $[111]$ lattice direction. The other two lines represent the resonances due to the unparallel NV^- defects having an axis in the lattice direction $[\bar{1}11]$, $[1\bar{1}1]$, or $[11\bar{1}]$.

III. NEAR THE LEVEL ANTICROSSING

Let ω_a denote the angular frequency ω_- corresponding to the NV^- defects with an axis in the $[111]$ lattice direction. Consider the case where the magnitude B_S of the solenoid field \mathbf{B}_S is tuned close to the value $D/\gamma_e = 102$ mT. In the vicinity of this level anticrossing point (LAC) the angular frequency ω_a is approximately given by $\omega_a = \omega_{a0} \sqrt{1 + \eta^2}$, where $\omega_{a0} = \sqrt{2D}\theta_S$ is the lowest value of the angular frequency ω_a , $\theta_S \ll 1$ is the angle between \mathbf{B}_S and the lattice direction $[111]$ ($\theta_S = 1.5^\circ$ and $\omega_{a0}/2\pi = 110$ MHz for the data shown in Figs. 2, 3, and 4), and the dimensionless detuning η is given by $\eta = \gamma_e \delta B_S / \omega_{a0}$, where $\delta B_S = B_S - D/\gamma_e$.

Measured ODMR near the LAC vs magnetic field B_S and driving frequency $f_{LA} = \omega_{LA}/2\pi$ of the signal injected into the loop antenna is seen in Fig. 3(a). The overlaid gray dashed lines are hyperbolas calculated according to $f_{LA} = f_l$, where the frequency of the l th hyperbola f_l is given by

$$f_l = \omega_a / 2\pi l = \omega_{a0} \sqrt{1 + \eta^2} / 2\pi l, \quad (3)$$

where l is an integer from 1 to 10. As can be seen from Fig. 3, along the l th hyperbola the largest signal is obtained when the driving frequency is tuned close to $\omega_c/2\pi l$, where

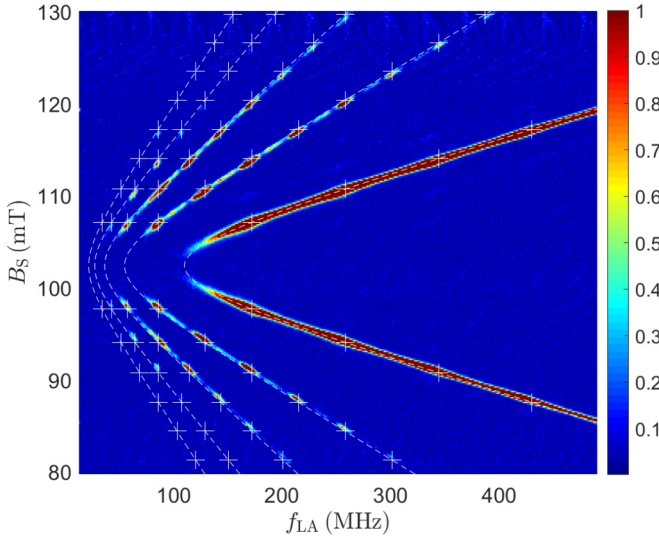


FIG. 4. ODMR with high laser power. The overlaid hyperbolas are calculated according to Eq. (3), and the locations of the crosses are calculated according to Eq. (6).

$\omega_c/2\pi = 276$ MHz is the cavity resonance frequency. This suggests that the spin MPRs are enhanced due to the interaction with the cavity mode.

IV. CAVITY SUPERHARMONIC RESONANCES

The effect of the coupled cavity mode on the spin MPR is discussed in the Appendix. The theoretical model presented in the Appendix describes the interplay between two mechanisms. The first one is frequency mixing between transverse and longitudinal spin driving. Near the avoided crossing point the NV^- spin states with magnetic quantum numbers -1 and 0 are mixed, and consequently, the amplitudes of transverse and longitudinal driving become strongly dependent on detuning from the avoided crossing point (even when the external driving is kept unchanged). The highly nonlinear nature of the first mechanism results in the generation of harmonics of the externally applied driving frequency. The second mechanism is cavity resonance enhancement, which becomes efficient when one of the generated harmonics coincides with the cavity resonance band. Under appropriate conditions this may give rise to a pronounced cavity-assisted multiphoton resonance.

Consider the case where the frequency of excitation injected into the loop antenna is tuned close to the l th superharmonic resonance, i.e., $\omega_a \simeq l\omega_{LA}$, where l is an integer. In that region, the relative change $P_z/P_{z,s}$ in spin polarization in the NV^- triplet ground state is found to be given by [see Eq. (A33) in the Appendix]

$$\frac{P_z}{P_{z,s}} = 1 - \frac{\beta_{\Delta}^2 |\zeta|^2}{1 + \beta_{\Delta}^2 |\zeta|^2 + \beta_{al}^2}, \quad (4)$$

where [see Eq. (A43)]

$$\zeta = J_l \left(\frac{\omega_b}{\omega_L} \right) \left(1 + \frac{\kappa J_0^2 \left(\frac{\omega_b}{\omega_L} \right) P_{z,s}}{(1 + i\beta_{cl})(1 + i\beta_{al})} \right), \quad (5)$$

ω_b is the amplitude of longitudinal spin driving [see Eq. (A8)], the dimensionless coupling coefficient β_{Δ} is given by $\beta_{\Delta} = \omega_{\Delta}/\sqrt{\gamma_1\gamma_2}$, the dimensionless detuning coefficients β_{cl} and β_{al} are given by $\beta_{cl} = (\omega_c - l\omega_{LA})/\gamma_c$ and $\beta_{al} = (\omega_a - l\omega_{LA})/\gamma_2$, respectively, ω_c is the cavity-mode angular frequency, γ_c is the cavity-mode damping rate, γ_1 and γ_2 are the longitudinal and transverse spin damping rates, respectively, and $\kappa = g^2/\gamma_2\gamma_c$ is the cooperativity parameter. A plot of the normalized steady-state polarization $P_z/P_{z,s}$ given by Eq. (4) is shown in Fig. 3(b). The comparison between data and theory yields qualitative agreement.

V. P1

ODMR data near the LAC with relatively high laser power are shown in Fig. 4. The increase in laser power gives rise to excessive heating, and consequently, the superconducting resonator mode becomes undetectable (in a microwave reflectivity measurement) due to a superconduction to normal-conduction phase transition of the spiral. The plot contains a variety of peaks all occurring along the above-discussed hyperbolas [see Eq. (3)], suggesting that some multiphoton processes continue to exist regardless of the spiral resonator state. Locations of all data peaks are determined by a single-frequency denoted by f_m . This can be seen from the cross symbols added to Fig. 4. The frequency $f_{k,l}$ of the k th cross symbol overlaid on the l th hyperbola in Fig. 4 is given by

$$f_{k,l} = \frac{k}{l} f_m, \quad (6)$$

where the frequency f_m takes the value $f_m = 86$ MHz. This pattern of peaks remains visible with the same value of f_m over a wide range of input microwave power (between 10 and 25 dBm), tenfold laser power attenuation, few-degree magnetic-field misalignments, and temperature change. With temperature rising to 30 K, the signal from the higher-order hyperbolas disappears, but the f_m beating remains on the main hyperbola. The fact that some of the peaks do not appear at the same frequency for different magnetic fields validates that the pattern is not a measurement artifact of spurious resonances. In addition, the synthesizer signal harmonics were carefully examined with a spectrum analyzer to verify they are all well below the ODMR sensitivity threshold. The measured value of f_m suggests a connection between MPRs in the NV^- defects and P1 defect [61–64], as is discussed below.

The P1 defect has four locally stable configurations. In each configuration a static Jahn-Teller distortion occurs, and an unpaired electron is shared by the nitrogen atom and by one of the four neighboring carbon atoms, which are positioned along one of the lattice directions $[111]$, $[\bar{1}11]$, $[1\bar{1}1]$, and $[11\bar{1}]$ [20,46,53,54,65–69].

When both nuclear Zeeman shift and nuclear quadrupole coupling are disregarded, the spin Hamiltonian of a P1 defect is given by [20,63,70] $\mathcal{H} = \gamma_e \mathbf{B} \cdot \mathbf{S} + \hbar^{-1} A_{\perp} (S_x I_x + S_y I_y) + \hbar^{-1} A_{\parallel} S_z I_z$, where $\mathbf{S} = (S_x, S_y, S_z)$ is an electronic spin-1/2 vector operator, $\mathbf{I} = (I_x, I_y, I_z)$ is a nuclear spin-1 vector operator, $A_{\parallel} = 2\pi \times 114.03$ MHz and $A_{\perp} = 2\pi \times 81.33$ MHz are, respectively, the longitudinal and transverse hyperfine parameters, and the z direction corresponds to the diamond $\langle 111 \rangle$ axis. The electron spin resonance at angular

frequency $\gamma_e B$ is split due to the interaction with the nuclear spin into three resonances, corresponding to three transitions, in which the nuclear-spin magnetic quantum number is conserved [27,52,55,65,71,72]. For a magnetic field larger than a few milliteslas the angular resonance frequencies are approximately given by $\gamma_e B$ and $\gamma_e B \pm \omega_{\text{en}}$, where $\omega_{\text{en}}^2 = A_{\parallel}^2 \cos^2 \theta_B + A_{\perp}^2 \sin^2 \theta_B$ and where θ_B is the angle between the magnetic field \mathbf{B} and the P1 axis [61].

Consider the case where \mathbf{B} is in the lattice direction [111]. For this case, for 1/4 of the P1 defects $\omega_{\text{en}} = 2\pi \times 114$ MHz, whereas for the other 3/4 of the P1 defects (unparallel to \mathbf{B} having an axis in one of the lattice directions $[\bar{1}11]$, $[1\bar{1}1]$, and $[11\bar{1}]$) $\omega_{\text{en}} = 2\pi \times 85.6$ MHz, close to the observed value of the frequency $f_m = 86$ MHz. The fact that the parallel P1 defects do not have a significant effect on the ODMR data can be attributed to the fact that these defects generate only transverse driving for the NV^- defects with an axis parallel to the crystal direction [111], whereas the unparallel P1 defects generate both transverse and longitudinal drivings, which in turn allow nonlinear processes of frequency mixing [73].

The effect of dipolar interactions on the measured ODMR signal can be estimated using perturbation theory. To first order the above-discussed hyperfine splitting has no effect. However, as is argued below, a nonvanishing effect is obtained from the second order. Consider a pair of P1 defects with a dipolar coupling to a single NV^- defect [74–80]. Both P1 defects are assumed to be unparallel to \mathbf{B} ; that is, the frequencies of their electroniclike transitions are approximately given by $\gamma_e B/2\pi$ and $\gamma_e B/2\pi \pm 85.6$ MHz. The NV^- defect, on the other hand, is assumed to be nearly parallel to \mathbf{B} , thus having an energy separation of $2\hbar\gamma_e B$ between the spin states with magnetic number ± 1 .

OISP polarizes the NV^- to the $m_s = 0$ state. The required condition for the ODMR signal along the l th hyperbola is achieved by excitation at $\omega_{\text{LA}} = \omega_a/l$, populating the $m_s = -1$ state, which has lower photoluminescence. Let $(m_s^{\text{NV}}, m_s^{\text{P1a}} + m_s^{\text{P1b}}, m_1^{\text{P1a}} + m_1^{\text{P1b}})$ designate a subspace, where m_s^{NV} is the NV^- electronic-spin magnetic number, m_s^{P1a} (m_s^{P1b}) is the first (second) P1 electronic-spin magnetic number, and m_1^{P1a} (m_1^{P1b}) is the first (second) P1 nuclear-spin magnetic number. Note that subspaces $(-1, +1, j)$ and $(+1, -1, j)$ for $j \in \{-2, -1, 0, 1, 2\}$ are energetically separated by $\hbar|j|\omega_{\text{en}}$. When $\omega_a = k\omega_{\text{en}}$ for integer k , transitions are stimulated between $(-1, +1, j)$ and $(+1, -1, j)$, further reducing the population of $(0, +1, j)$ and consequently enhancing the ODMR signal.

By employing perturbation theory [81] we find that the effective Rabi rate for these tripolar transitions is roughly given by $\omega_{\text{P1P1NV}} \simeq (n_{\text{S,P1}}/n_{\text{D}})^2 D$, where $n_{\text{S,P1}}$ is the density of P1 defects (which is assumed to be about 100 times larger than the density of NV^- defects and which can be expressed in terms of the relative concentration of nitrogen atoms p_{N} as $n_{\text{S,P1}} = 1.8 \times 10^{23} \text{ cm}^{-3} p_{\text{N}}$) and where $n_{\text{D}} = 4\pi D/\mu_0\gamma_e^2\hbar = 5.5 \times 10^{22} \text{ cm}^{-3}$. The roughly estimated value of $p_{\text{N}} = 10^{-4}$ yields the rate $\omega_{\text{P1P1NV}}/2\pi \simeq 300$ Hz. In a similar setup [57], at $T = 3.5$ K the maximal OISP rate was found to be $T_{\text{O}}^{-1} \approx 200$ Hz and $\gamma_1 \approx 25$ Hz; hence this mechanism is expected to be significant to a low-temperature ODMR measurement.

Note that the transition between $(-1, +1, 0)$ and $(+1, -1, 0)$ does not require additional energy. Stimulated

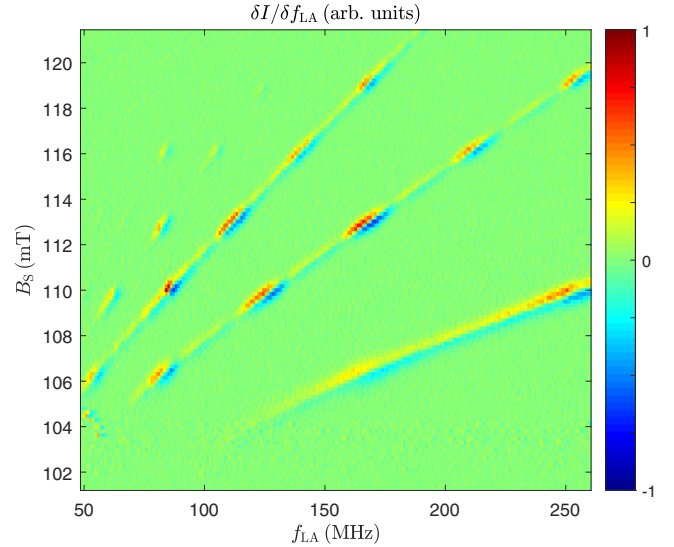


FIG. 5. Derivative of the ODMR photoluminescence signal I with respect to the driving signal frequency f_{LA} at high laser power. The absolute maximal values are achieved not along the single-photon curve (bottom right diagonal), but rather at the spots attributed to P1 hyperfine processes on the NV MPR curves (top left diagonals).

nuclear-spin rotation with $\omega_a = k\omega_{\text{en}}/2$ for integer k allows population of $(+1, -1, j_1)$ for $j_1 \in \{-2, -1, 1, 2\}$ via processes of sequential photon absorption. This effect gives rise to the weak peaks on the second ($l = 2$) hyperbola in Fig. 4.

The MPR can be employed to enhance the responsivity of diamond-based magnetometry. Consider a setup with a small frequency modulation about a central frequency f_{LA} and photoluminescence signal I demodulation readout. To maximize the responsivity, the bias magnetic field B_{S} and f_{LA} should be set to maximize the derivative $|dI/df_{\text{LA}}|$. As can be seen in Fig. 5, $|dI/df_{\text{LA}}|$ is maximal near the spots associated with P1 hyperfine transitions at the MPR of NV. This enhancement is attributed to the relatively narrow resonance of the P1 process compared to the NV MPR.

VI. SUMMARY

Multiphoton processes are surprisingly very measurable in Ib diamonds, making this mode of operation preferable for enhanced sensitivity in multiple applications. Of particular interest is the interaction of the optically measurable and polarizable NV ensemble with the naturally occurring P1 ensemble. The unexpected strength of coupling to the hyperfine transitions of the P1 requires further investigation to determine the nature of the interaction. The NV defects can potentially provide optical access to a much denser and coherent (nuclear) ensemble of the P1.

ACKNOWLEDGMENT

We greatly appreciate fruitful discussions with P. London, A. Blank, E. Lifshitz, V. Dyakonov, S. Tarasenko, V. Soltaimov, N. Katz, M. Stern, and N. Bar-Gil.

APPENDIX: DRIVEN SPINS COUPLED TO A RESONATOR

Consider a cavity mode coupled to a spin ensemble. The Hamiltonian of the closed system is taken to be given by

$$\hbar^{-1}\mathcal{H}_0 = \omega_c A^\dagger A + \frac{\boldsymbol{\Omega} \cdot \boldsymbol{\Sigma}}{2} + g(A\Sigma_+ + A^\dagger\Sigma_-), \quad (\text{A1})$$

where ω_c is the cavity-mode angular frequency, $A^\dagger A$ is a cavity-mode number operator, $\boldsymbol{\Sigma} = (\Sigma_x, \Sigma_y, \Sigma_z)$, and the spin operators Σ_z , $\Sigma_+ = (\Sigma_x + i\Sigma_y)/2$ and $\Sigma_- = (\Sigma_x - i\Sigma_y)/2$ are related to the eigenvectors $|\pm\rangle$ of the operator Σ_z by

$$\Sigma_z = |+\rangle\langle+| - |-\rangle\langle-|, \quad (\text{A2})$$

$$\Sigma_+ = |+\rangle\langle-|, \quad (\text{A3})$$

$$\Sigma_- = |-\rangle\langle+|. \quad (\text{A4})$$

The effective magnetic field $\boldsymbol{\Omega}(t)$ is expressed in terms of the angular frequency ω_T and amplitude ω_1 of transverse driving, the longitudinal magnetic-field component $\omega_0(t)$, and the transverse one ω_Δ

$$\boldsymbol{\Omega}(t) = \omega_1[\cos(\omega_T t)\hat{\mathbf{x}} + \sin(\omega_T t)\hat{\mathbf{y}}] + \omega_0\hat{\mathbf{z}} + \omega_\Delta\hat{\mathbf{x}} \quad (\text{A5})$$

or

$$\begin{aligned} \boldsymbol{\Omega}(t) = & \omega_1(e^{-i\omega_T t}\hat{\mathbf{u}}_+ + e^{i\omega_T t}\hat{\mathbf{u}}_-) + \omega_0(t)\hat{\mathbf{z}} \\ & + \omega_\Delta(\hat{\mathbf{u}}_+ + \hat{\mathbf{u}}_-), \end{aligned} \quad (\text{A6})$$

where ω_Δ is a real constant and

$$\hat{\mathbf{u}}_\pm = (1/2)(\hat{\mathbf{x}} \pm i\hat{\mathbf{y}}). \quad (\text{A7})$$

While ω_1 and ω_T are both assumed to be real constants, ω_0 is allowed to vary in time according to

$$\omega_0 = \omega_a - \omega_b \sin(\omega_L t), \quad (\text{A8})$$

where ω_a , ω_b , and ω_L are all real constants.

The Bose

$$[A, A^\dagger] = 1 \quad (\text{A9})$$

and spin

$$[\Sigma_z, \Sigma_+] = 2\Sigma_+, \quad (\text{A10})$$

$$[\Sigma_z, \Sigma_-] = -2\Sigma_-, \quad (\text{A11})$$

$$[\Sigma_+, \Sigma_-] = \Sigma_z \quad (\text{A12})$$

commutation relations are assumed to hold. The Heisenberg equations of motion are generated according to

$$\frac{dO}{dt} = -i[O, \hbar^{-1}\mathcal{H}_0], \quad (\text{A13})$$

where O is an operator; hence

$$\frac{dA}{dt} = -i\omega_c A - ig\Sigma_-, \quad (\text{A14})$$

$$\frac{d\Sigma_z}{dt} = W_1\Sigma_+ + W_1^\dagger\Sigma_-, \quad (\text{A15})$$

and

$$\frac{d\Sigma_+}{dt} = i\omega_0\Sigma_+ - \frac{W_1^\dagger}{2}\Sigma_z, \quad (\text{A16})$$

where

$$W_1 = -i(\omega_1 e^{-i\omega_T t} + \omega_\Delta + 2gA). \quad (\text{A17})$$

Averaging

$$\langle A \rangle = \alpha, \quad (\text{A18})$$

$$\langle \Sigma_z \rangle = P_z, \quad (\text{A19})$$

$$\langle \Sigma_\pm \rangle = P_\pm \quad (\text{A20})$$

and introducing damping lead to

$$\frac{d\alpha}{dt} = -(i\omega_c + \gamma_c)\alpha - igP_-, \quad (\text{A21})$$

$$\frac{dP_z}{dt} = \Omega_1 P_+ + \Omega_1^* P_- - \gamma_1(P_z - P_{z,s}), \quad (\text{A22})$$

and

$$\frac{dP_+}{dt} = i\omega_0 P_+ - \frac{\Omega_1^*}{2} P_z - \gamma_2 P_+, \quad (\text{A23})$$

where γ_c is the cavity-mode damping rate, γ_1 and γ_2 are the longitudinal and transverse spin damping rates, respectively, and

$$\Omega_1 = -i(\omega_1 e^{-i\omega_T t} + \omega_\Delta + 2g\alpha). \quad (\text{A24})$$

For our experimental conditions the term proportional to ω_1 in Eq. (A24) can be disregarded.

The effect of OISP can be accounted for by adjusting the values of the longitudinal damping rate γ_1 and steady-state polarization $P_{z,s}$ and making them both dependent on laser intensity [23,32]. In this approach γ_1 is given by $\gamma_1 = \gamma_{1T} + \gamma_{1O}$, where γ_{1T} is the rate of thermal relaxation and γ_{1O} is the rate of OISP (proportional to laser intensity), and the averaged value of steady-state polarization $P_{z,s}$ is given by

$$P_{z,s} = \frac{\gamma_{1T} P_{z,ST} + \gamma_{1O} P_{z,SO}}{\gamma_1}. \quad (\text{A25})$$

While $P_{z,ST}$ represents the steady-state polarization in the limit $\gamma_{1T} \gg \gamma_{1O}$ (i.e., when OISP is negligibly small), the value is $P_{z,SO}$ for the other extreme case of $\gamma_{1O} \gg \gamma_{1T}$ (i.e., when thermal relaxation is negligibly small).

By employing the transformation

$$P_+ = e^{i\theta_d} P_{d+}, \quad (\text{A26})$$

where

$$\theta_d = \int^t dt' [\omega_0(t') + \Delta] \quad (\text{A27})$$

and Δ is a real constant (to be determined later), Eqs. (A21), (A22), and (A23) become

$$\frac{d\alpha}{dt} = -(i\omega_c + \gamma_c)\alpha - ig\left(\frac{\omega_\Delta \zeta}{\Omega_1}\right)^* P_{d+}^*, \quad (\text{A28})$$

$$\frac{dP_z}{dt} = \omega_\Delta(\zeta P_{d+} + \zeta^* P_{d+}^*) - \gamma_1(P_z - P_{z,s}), \quad (\text{A29})$$

and

$$\frac{dP_{d+}}{dt} = -i\Delta P_{d+} - \frac{\omega_\Delta \zeta^*}{2} P_z - \gamma_2 P_{d+}, \quad (\text{A30})$$

where

$$\zeta = \frac{\Omega_1}{\omega_\Delta} e^{i\theta_d}. \quad (\text{A31})$$

When ζ is treated as a constant, the steady-state solution of Eqs. (A29) and (A30) reads

$$P_{d+} = \frac{\omega_\Delta \zeta^* P_z}{2(-i\Delta - \gamma_2)} \quad (\text{A32})$$

and

$$\frac{P_z}{P_{z,s}} = 1 - \frac{\frac{|\omega_\Delta \zeta|^2}{\gamma_1 \gamma_2}}{1 + \frac{|\omega_\Delta \zeta|^2}{\gamma_1 \gamma_2} + \frac{\Delta^2}{\gamma_2^2}}. \quad (\text{A33})$$

With the help of the Jacobi-Anger expansion, which is given by

$$\exp(iz \cos \theta) = \sum_{n=-\infty}^{\infty} i^n J_n(z) e^{in\theta}, \quad (\text{A34})$$

one obtains [see Eqs. (A8) and (A31)]

$$\zeta = \frac{\Omega_1}{\omega_\Delta} e^{-\frac{i\omega_b}{\omega_L}} \sum_{l'=-\infty}^{\infty} i^{l'} J_{l'}\left(\frac{\omega_b}{\omega_L}\right) e^{i(\omega_a + \Delta + l'\omega_L)t}. \quad (\text{A35})$$

Consider the case where $\omega_a \simeq l\omega_L$, where l is an integer. For this case the detuning Δ is chosen to be given by $\Delta = l\omega_L - \omega_a$, and consequently, ζ becomes

$$\zeta = \frac{\Omega_1}{\omega_\Delta} e^{-\frac{i\omega_b}{\omega_L}} \sum_{l'=-\infty}^{\infty} i^{l'} J_{l'}\left(\frac{\omega_b}{\omega_L}\right) e^{i(l+l')\omega_L t}. \quad (\text{A36})$$

The driving term of Eq. (A28) $-ig(\omega_\Delta \zeta / \Omega_1)^* P_{d+}^*$ is approximated by keeping only the term $l' = 0$ in Eq. (A36). When P_{d+}^* is treated as a constant, Eq. (A28) yields a steady-state solution given by $\alpha = \alpha_0 e^{-il\omega_L t}$, where

$$\alpha_0 = -\frac{ig e^{\frac{i\omega_b}{\omega_L}} J_0\left(\frac{\omega_b}{\omega_L}\right) P_{d+}^*}{\gamma_c (1 + i\beta_{cl})} \quad (\text{A37})$$

and

$$\beta_{cl} = \frac{\omega_c - l\omega_L}{\gamma_c}. \quad (\text{A38})$$

To lowest nonvanishing order in the coupling g the coefficient P_{d+}^* in Eq. (A37) is evaluated using Eq. (A32) by keeping only the term $l' = -l$ in Eq. (A36) and keeping only the term $-i\omega_\Delta$ in Eq. (A24),

$$P_{d+}^* = \frac{i^{1-l} e^{-\frac{i\omega_b}{\omega_L}} \omega_\Delta J_{-l}\left(\frac{\omega_b}{\omega_L}\right) P_{z,s}}{2\gamma_2 (1 + i\beta_{al})}, \quad (\text{A39})$$

where

$$\beta_{al} = \frac{\omega_a - l\omega_L}{\gamma_2}, \quad (\text{A40})$$

and thus [see Eq. (A37)]

$$\alpha_0 = -\frac{i^{2-l} g \omega_\Delta J_0\left(\frac{\omega_b}{\omega_L}\right) J_{-l}\left(\frac{\omega_b}{\omega_L}\right) P_{z,s}}{\gamma_c \gamma_2 2(1 + i\beta_{cl})(1 + i\beta_{al})}. \quad (\text{A41})$$

It is assumed that the dominant contribution of ζ to the equation of motion (A29) and (A30) comes from a term labeled ζ_a , which is given by [see Eqs. (A24) and (A36)]

$$i e^{\frac{i\omega_b}{\omega_L}} \zeta_a = i^{-l} J_{-l}\left(\frac{\omega_b}{\omega_L}\right) + \frac{2g\alpha_0}{\omega_\Delta} J_0\left(\frac{\omega_b}{\omega_L}\right). \quad (\text{A42})$$

With the help of Eq. (A41) this becomes

$$i^{1+l} e^{\frac{i\omega_b}{\omega_L}} \zeta_a = J_{-l}\left(\frac{\omega_b}{\omega_L}\right) \left(1 + \frac{\kappa J_0^2\left(\frac{\omega_b}{\omega_L}\right) P_{z,s}}{(1 + i\beta_{cl})(1 + i\beta_{al})}\right), \quad (\text{A43})$$

where the cooperativity parameter κ is given by

$$\kappa = \frac{g^2}{\gamma_2 \gamma_c}. \quad (\text{A44})$$

The above results (A33) and (A43) lead to Eq. (4) in the main text for the steady-state polarization.

-
- [1] J. H. Shirley, *Phys. Rev.* **138**, B979 (1965).
 [2] D. M. Berns, W. D. Oliver, S. O. Valenzuela, A. V. Shytov, K. K. Berggren, L. S. Levitov, and T. P. Orlando, *Phys. Rev. Lett.* **97**, 150502 (2006).
 [3] R. Tycko and S. Opella, *J. Chem. Phys.* **86**, 1761 (1987).
 [4] F. H. Faisal, *Theory of Multiphoton Processes* (Springer, Berlin, 2013).
 [5] L. Childress and J. McIntyre, *Phys. Rev. A* **82**, 033839 (2010).
 [6] H. Y. Chen, E. R. MacQuarrie, and G. D. Fuchs, *Phys. Rev. Lett.* **120**, 167401 (2018).
 [7] H. J. Mamin, M. H. Sherwood, M. Kim, C. T. Rettner, K. Ohno, D. D. Awschalom, and D. Rugar, *Phys. Rev. Lett.* **113**, 030803 (2014).
 [8] B. Mollow, in *Coherence and Quantum Optics* (Springer, Berlin, 1973), pp. 525–532.
 [9] H. Freedhoff and T. Quang, *Phys. Rev. Lett.* **72**, 474 (1994).
 [10] J. Weber, *Rev. Mod. Phys.* **31**, 681 (1959).
 [11] M. A. Armen and H. Mabuchi, *Phys. Rev. A* **73**, 063801 (2006).
 [12] F. Grossmann, T. Dittrich, P. Jung, and P. Hänggi, *Phys. Rev. Lett.* **67**, 516 (1991).
 [13] H. Lignier, C. Sias, D. Ciampini, Y. Singh, A. Zenesini, O. Morsch, and E. Arimondo, *Phys. Rev. Lett.* **99**, 220403 (2007).
 [14] G. D. Fuchs, V. V. Dobrovitski, D. M. Toyli, F. J. Heremans, and D. D. Awschalom, *Science* **326**, 1520 (2009).
 [15] M. W. Doherty, N. B. Manson, P. Delaney, F. Jelezko, J. Wrachtrup, and L. C. Hollenberg, *Phys. Rep.* **528**, 1 (2013).

- [16] X. Zhu, S. Saito, A. Kemp, K. Kakuyanagi, S.-i. Karimoto, H. Nakano, W. J. Munro, Y. Tokura, M. S. Everitt, K. Nemoto *et al.*, *Nature (London)* **478**, 221 (2011).
- [17] Y. Kubo, F. R. Ong, P. Bertet, D. Vion, V. Jacques, D. Zheng, A. Dréau, J.-F. Roch, A. Auffeves, F. Jelezko, J. Wrachtrup, M. F. Barthe, P. Bergonzo, and D. Esteve, *Phys. Rev. Lett.* **105**, 140502 (2010).
- [18] Y. Kubo, C. Grezes, A. Dewes, T. Umeda, J. Isoya, H. Sumiya, N. Morishita, H. Abe, S. Onoda, T. Ohshima *et al.*, *Phys. Rev. Lett.* **107**, 220501 (2011).
- [19] R. Amsüss, C. Koller, T. Nöbauer, S. Putz, S. Rotter, K. Sandner, S. Schneider, M. Schramböck, G. Steinhauser, H. Ritsch *et al.*, *Phys. Rev. Lett.* **107**, 060502 (2011).
- [20] D. I. Schuster, A. P. Sears, E. Ginossar, L. DiCarlo, L. Frunzio, J. J. L. Morton, H. Wu, G. A. D. Briggs, B. B. Buckley, D. D. Awschalom, and R. J. Schoelkopf, *Phys. Rev. Lett.* **105**, 140501 (2010).
- [21] K. Sandner, H. Ritsch, R. Amsüss, C. Koller, T. Nöbauer, S. Putz, J. Schmiedmayer, and J. Majer, *Phys. Rev. A* **85**, 053806 (2012).
- [22] C. Grezes, B. Julsgaard, Y. Kubo, M. Stern, T. Umeda, J. Isoya, H. Sumiya, H. Abe, S. Onoda, T. Ohshima *et al.*, *Phys. Rev. X* **4**, 021049 (2014).
- [23] N. Alfasi, S. Masis, R. Winik, D. Farfurnik, O. Shtempluck, N. Bar-Gill, and E. Buks, *Phys. Rev. A* **97**, 063808 (2018).
- [24] G. A. Álvarez, C. O. Bretschneider, R. Fischer, P. London, H. Kanda, S. Onoda, J. Isoya, D. Gershoni, and L. Frydman, *Nat. Commun.* **6**, 8456 (2015).
- [25] E. J. Kamp, B. Carvajal, and N. Samarth, *Phys. Rev. B* **97**, 045204 (2018).
- [26] A. O. Sushkov, I. Lovchinsky, N. Chisholm, R. L. Walsworth, H. Park, and M. D. Lukin, *Phys. Rev. Lett.* **113**, 197601 (2014).
- [27] C. Belthangady, N. Bar-Gill, L. M. Pham, K. Arai, D. Le Sage, P. Cappellaro, and R. L. Walsworth, *Phys. Rev. Lett.* **110**, 157601 (2013).
- [28] M. W. Doherty, F. Dolde, H. Fedder, F. Jelezko, J. Wrachtrup, N. B. Manson, and L. C. L. Hollenberg, *Phys. Rev. B* **85**, 205203 (2012).
- [29] G. Balasubramanian, P. Neumann, D. Twitchen, M. Markham, R. Kolesov, N. Mizuochi, J. Isoya, J. Achard, J. Beck, J. Tissler *et al.*, *Nat. Mater.* **8**, 383 (2009).
- [30] L. Robledo, H. Bernien, T. van der Sar, and R. Hanson, *New J. Phys.* **13**, 025013 (2011).
- [31] D. A. Redman, S. Brown, R. H. Sands, and S. C. Rand, *Phys. Rev. Lett.* **67**, 3420 (1991).
- [32] C. S. Shin, C. E. Avalos, M. C. Butler, D. R. Trease, S. J. Seltzer, J. P. Mustonen, D. J. Kennedy, V. M. Acosta, D. Budker, A. Pines *et al.*, *J. Appl. Phys.* **112**, 124519 (2012).
- [33] R. Chapman and T. Plakhotnik, *Chem. Phys. Lett.* **507**, 190 (2011).
- [34] A. Gruber, A. Dräbenstedt, C. Tietz, L. Fleury, J. Wrachtrup, and C. Von Borczyskowski, *Science* **276**, 2012 (1997).
- [35] J. Maze, P. Stanwix, J. Hodges, S. Hong, J. Taylor, P. Cappellaro, L. Jiang, M. G. Dutt, E. Togan, A. Zibrov *et al.*, *Nature (London)* **455**, 644 (2008).
- [36] V. M. Acosta, E. Bauch, M. P. Ledbetter, A. Waxman, L.-S. Bouchard, and D. Budker, *Phys. Rev. Lett.* **104**, 070801 (2010).
- [37] G. Balasubramanian, I. Chan, R. Kolesov, M. Al-Hmoud, J. Tisler, C. Shin, C. Kim, A. Wojcik, P. R. Hemmer, A. Krueger *et al.*, *Nature (London)* **455**, 648 (2008).
- [38] T. Wolf, P. Neumann, K. Nakamura, H. Sumiya, T. Ohshima, J. Isoya, and J. Wrachtrup, *Phys. Rev. X* **5**, 041001 (2015).
- [39] H. Mamin, M. Kim, M. Sherwood, C. Rettner, K. Ohno, D. Awschalom, and D. Rugar, *Science* **339**, 557 (2013).
- [40] M. Pelliccione, A. Jenkins, P. Ovarthaiyapong, C. Reetz, E. Emmanouilidou, N. Ni, and A. C. B. Jayich, *Nat. Nanotechnol.* **11**, 700 (2016).
- [41] L. Rondin, J.-P. Tetienne, S. Rohart, A. Thiaville, T. Hingant, P. Spinicelli, J.-F. Roch, and V. Jacques, *Nat. Commun.* **4**, 2279 (2013).
- [42] F. Dolde, H. Fedder, M. W. Doherty, T. Nöbauer, F. Rempp, G. Balasubramanian, T. Wolf, F. Reinhard, L. Hollenberg, F. Jelezko *et al.*, *Nat. Phys.* **7**, 459 (2011).
- [43] F. Jelezko, T. Gaebel, I. Popa, A. Gruber, and J. Wrachtrup, *Phys. Rev. Lett.* **92**, 076401 (2004).
- [44] P. C. Maurer, G. Kucsko, C. Latta, L. Jiang, N. Y. Yao, S. D. Bennett, F. Pastawski, D. Hunger, N. Chisholm, M. Markham *et al.*, *Science* **336**, 1283 (2012).
- [45] J. Cai, F. Jelezko, N. Katz, A. Retzker, and M. B. Plenio, *New J. Phys.* **14**, 093030 (2012).
- [46] S. Takahashi, R. Hanson, J. van Tol, M. S. Sherwin, and D. D. Awschalom, *Phys. Rev. Lett.* **101**, 047601 (2008).
- [47] R. Fischer, C. O. Bretschneider, P. London, D. Budker, D. Gershoni, and L. Frydman, *Phys. Rev. Lett.* **111**, 057601 (2013).
- [48] R. Fischer, A. Jarmola, P. Kehayias, and D. Budker, *Phys. Rev. B* **87**, 125207 (2013).
- [49] H.-J. Wang, C. S. Shin, C. E. Avalos, S. J. Seltzer, D. Budker, A. Pines, and V. S. Bajaj, *Nat. Commun.* **4**, 1940 (2013).
- [50] I. Solomon, *Phys. Rev.* **99**, 559 (1955).
- [51] M. Loretz, H. Takahashi, T. F. Segawa, J. M. Boss, and C. L. Degen, *Phys. Rev. B* **95**, 064413 (2017).
- [52] M. Simanovskaia, K. Jensen, A. Jarmola, K. Aulenbacher, N. Manson, and D. Budker, *Phys. Rev. B* **87**, 224106 (2013).
- [53] H. Clevenson, E. H. Chen, F. Dolde, C. Teale, D. Englund, and D. Braje, *Phys. Rev. A* **94**, 021401(R) (2016).
- [54] H.-J. Wang, C. S. Shin, S. J. Seltzer, C. E. Avalos, A. Pines, and V. S. Bajaj, *Nat. Commun.* **5**, 4135 (2014).
- [55] L. Hall, P. Kehayias, D. Simpson, A. Jarmola, A. Stacey, D. Budker, and L. Hollenberg, *Nat. Commun.* **7**, 10211 (2016).
- [56] C. M. Purser, V. P. Bhallamudi, C. S. Wolfe, H. Yusuf, B. A. McCullian, C. Jayaprakash, M. E. Flatté, and P. C. Hammel, *J. Phys. D: Appl. Phys.* **52**, 305004 (2019).
- [57] N. Alfasi, S. Masis, O. Shtempluck, and E. Buks, *Phys. Rev. B* **99**, 214111 (2019).
- [58] C. Kurter, A. P. Zhuravel, J. Abrahams, C. L. Bennett, A. V. Ustinov, and S. M. Anlage, *IEEE Trans. Appl. Supercond.* **21**, 709 (2011).
- [59] P. Ovarthaiyapong, K. W. Lee, B. A. Myers, and A. C. B. Jayich, *Nat. Commun.* **5**, 4429 (2014).
- [60] E. R. MacQuarrie, T. A. Gosavi, N. R. Jungwirth, S. A. Bhawe, and G. D. Fuchs, *Phys. Rev. Lett.* **111**, 227602 (2013).
- [61] W. Smith, P. Sorokin, I. Gelles, and G. Lasher, *Phys. Rev.* **115**, 1546 (1959).
- [62] R. Cook and D. Whiffen, *Proc. R. Soc. London, Ser. A* **295**, 99 (1966).
- [63] J. Loubser and J. van Wyk, *Rep. Prog. Phys.* **41**, 1201 (1978).
- [64] R. Barklie and J. Guven, *J. Phys. C* **14**, 3621 (1981).

- [65] R. Hanson, V. Dobrovitski, A. Feiguin, O. Gywat, and D. Awschalom, *Science* **320**, 352 (2008).
- [66] D. A. Broadway, J. D. Wood, L. T. Hall, A. Stacey, M. Markham, D. A. Simpson, J.-P. Tetienne, and L. C. L. Hollenberg, *Phys. Rev. Appl.* **6**, 064001 (2016).
- [67] J. H. Shim, B. Nowak, I. Niemeyer, J. Zhang, F. D. Brandao, and D. Suter, [arXiv:1307.0257](https://arxiv.org/abs/1307.0257).
- [68] B. Smeltzer, L. Childress, and A. Gali, *New J. Phys.* **13**, 025021 (2011).
- [69] C. S. Shin, M. C. Butler, H.-J. Wang, C. E. Avalos, S. J. Seltzer, R.-B. Liu, A. Pines, and V. S. Bajaj, *Phys. Rev. B* **89**, 205202 (2014).
- [70] J. D. A. Wood, D. A. Broadway, L. T. Hall, A. Stacey, D. A. Simpson, J.-P. Tetienne, and L. C. L. Hollenberg, *Phys. Rev. B* **94**, 155402 (2016).
- [71] C. P. Slichter, *Principles of Magnetic Resonance* (Springer, Berlin, 2013), Vol. 1.
- [72] E. van Oort, P. Stroomeer, and M. Glasbeek, *Phys. Rev. B* **42**, 8605 (1990).
- [73] C. Cohen-Tannoudji, J. Dupont-Roc, and G. Grynberg, *Atom-Photon Interactions: Basic Processes and Applications* (Wiley-VCH, New York, 1998).
- [74] R. Hanson, F. M. Mendoza, R. J. Epstein, and D. D. Awschalom, *Phys. Rev. Lett.* **97**, 087601 (2006).
- [75] A. Bermudez, F. Jelezko, M. B. Plenio, and A. Retzker, *Phys. Rev. Lett.* **107**, 150503 (2011).
- [76] M. Kohl, M. Odehnl, V. Petříček, R. Tichý, and S. Šafrata, *J. Low Temp. Phys.* **72**, 319 (1988).
- [77] H. Cheng, *Phys. Rev.* **124**, 1359 (1961).
- [78] J. Daycock and G. P. Jones, *J. Phys. C* **2**, 998 (1969).
- [79] B. Alekseev, *Radiophys. Quantum Electron.* **18**, 1272 (1975).
- [80] G. V. Varada and G. S. Agarwal, *Phys. Rev. A* **45**, 6721 (1992).
- [81] J. R. Schrieffer and P. A. Wolff, *Phys. Rev.* **149**, 491 (1966).